Data-Driven Personalization of Body-Machine Interfaces to Control Diverse Robot Types

Matteo Macchini (matteo.macchini@gmail.com)
Ecole Polytechnique Federale de Lausanne https://orcid.org/0000-0002-8744-4389
Fabrizio Schiano
Ecole Polytechnique Federale de Lausanne https://orcid.org/0000-0002-9472-5381
Dario Floreano
Ecole Polytechnique Federale de Lausanne https://orcid.org/0000-0002-5330-4863

Article

Keywords: Body-Machine Interfaces, robotic teleoperation, machine learning

Posted Date: July 8th, 2021

DOI: https://doi.org/10.21203/rs.3.rs-657990/v1

Data-Driven Personalization of Body-Machine Interfaces to Control Diverse Robot Types

Matteo Macchini[1,*], **Fabrizio Schiano**[1], **and Dario Floreano**[1]

[1]Laboratory of Intelligent Systems, École Polytechnique Fédérale de Lausanne, CH-1015 Lausanne (EPFL), Switzerland.
[*]matteo.macchini@epfl.ch

ABSTRACT

Body-Machine Interfaces (BoMIs) for robotic teleoperation can improve a user's experience and performance. However, the implementation of such systems needs to be optimized on each robot independently, as a general approach has not been proposed to date. Here, we present a novel machine learning method to generate personalized BoMIs from an operator's spontaneous body movements. The method captures individual motor synergies that can be used for the teleoperation of robots. The proposed algorithm applies to people with diverse behavioral patterns to control robots with diverse morphologies and degrees of freedom, such as a fixed-wing drone, a quadrotor, and a robotic manipulator

Introduction

Telerobotic systems play a fundamental role in several robotics applications, such as search-and-rescue, exploration, and manipulation tasks[1], where human perception and cognitive abilities cannot yet be matched in performance and reliability by machine intelligence[2–5]. In this context, human-robot interfaces (HRIs) should be easily learned and mastered by the human operator[6]. However, standard HRIs, such as joysticks, keyboards, and mice fail to provide efficient teleoperation of the robot for inexperienced users and require substantial effort and time to be mastered proficiently[7–9].

Body-Machine Interfaces (BoMIs) are a form of HRI that translate body motion into control commands and can be more intuitive in controlling a distal robot because they leverage spontaneous movements[10]. This approach has been successfully applied for the control of different devices such as wheelchairs[11,12] and mobile robots[13–15]. A BoMI requires the design of a mapping function that translates body motion into robot actions[16]. Currently, there is no standard method to define such mappings for motion-based BoMIs. Heuristic methods are based on gestures commonly adopted in human communication, such as pointing[17–20], or leverage kinematic correspondences between human and robot morphologies, for example by letting an operator control an anthropomorphic robotic arm using their arm motion[21,22]. Data-driven methods rely on data from human spontaneous motor behavior when interacting with the robot, and have been used to control aerial robots[10], ground robots[23] and humanoid manipulators[24].

Some of these works track only the body segments that resulted in the most commonly adopted for the control of the considered robot in a pilot study[10,20,25]. Others fix the body segments to be tracked without user studies and derive a mapping by regressing human motion data over robot's motion data[26,27]. Recently, we propose a method to identify a BoMI mapping that automatically identifies and uses human motion patterns to control a robot and we validated it in the teleoperation of a fixed-wing drone[28]. However, a problem with these methods is that they are tailored to a single robotic platform. Therefore, their transfer to different robots might fail, especially when the robots have different morphologies and degrees of freedom.

Human motion is organized in synergies, i.e. functional motor units requiring the coordinated action of several body segments[29]. Grasping an object or walking are everyday examples of motor synergies widely studied in the literature[30–32]. This synergistic organization of motion generates multicollinear datasets, where some variables can be dependent on each other[33]. Multicollinear datasets can lead to overfitting in regression models, which can in turn fail to identify the correct motion intended by the user and produce unusable HRIs. Several solutions have been proposed to solve this problem, including dimensionality reduction and regularization methods[34,35]. Some research works employ dimensionality reduction as the main processing step to implement BoMIs: by compressing the most relevant motion features, the user's motion and the device's inputs are paired[11,12,36,37]. However, a method capable of deriving Body-Machine Interfaces for different robots and different human motion patterns is still missing.

In this paper, we propose a novel machine learning algorithm designed to identify human motor synergies and translate them into robot commands. Our method allows inexperienced users to control diverse robots without prior training. We

validated the method with three real-world robots with an increasing number of Degrees of Freedom (DoFs): a fixed-wing drone with controllable speed (3 DoFs), a quadrotor with 4 DoF, and a 6-DoF manipulator. We assessed the effectiveness of the resulting personalized BoMIs by comparing them with standard remote controllers in a user study. Experimental results with simulated and real robots indicate that the proposed method based on the identification of motion synergies can generate effective personalized BoMIs for all the considered robots.

Experimental Setup

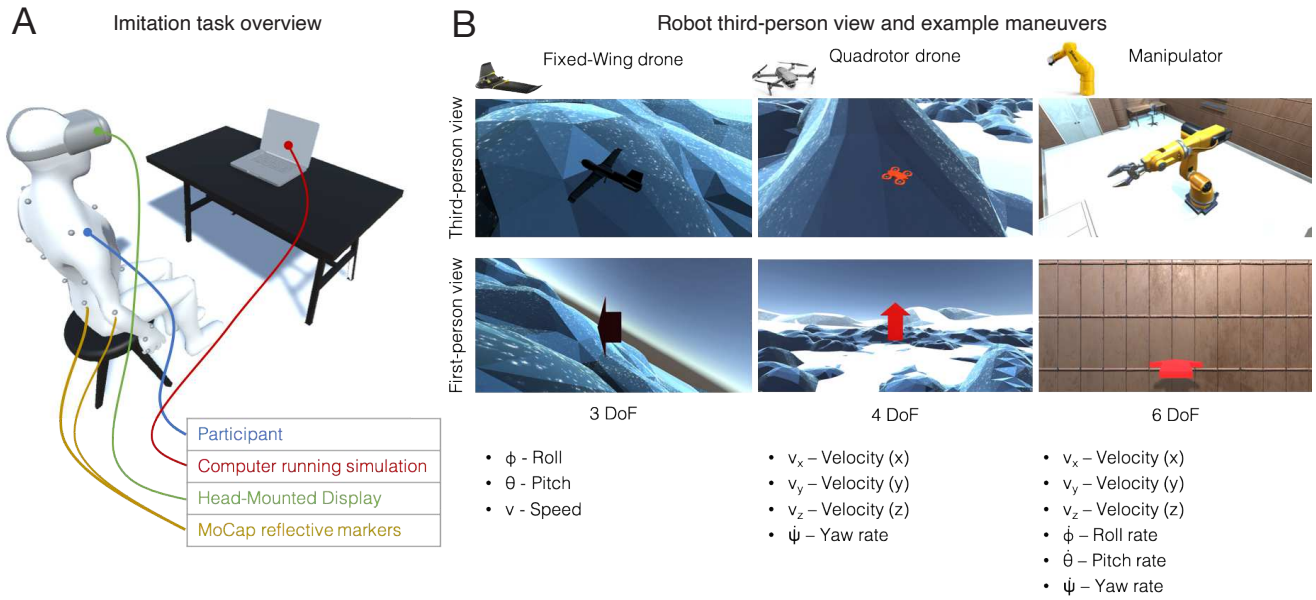

Figure 1. Motion acquisition scenario. (A) The participant sits in front of a computer simulating three different robots. The simulation is shown to them through an HMD while their body motion is tracked through a Motion Capture system. (B) We ensure that the participants know the robot they are controlling by showing the robot from a third-person view before moving to a first-person view. Each robot performs a set of predefined maneuvers spanning all its degrees of freedom. The robots were presented in the order fixed-wing, quadrotor, manipulator.

Identification of motion strategies

10 participants took part in an experiment aimed at identifying human motion strategies for the control of three robots: a fixed-wing drone, a quadrotor, and a robotic manipulator. The goal of this first experiment is twofold: first, we will observe common human motion patterns when interacting with different machines to investigate their nature and the need for personalized BoMIs, second, we will use the collected data to validate our method.

The participants were sitting on a stool, and presented with a First-Person View (FPV) of the robot motion through a camera mounted on its front (Fig. 1, Videos S1, S2, S3). The robots were simulated in Unity3D and the images were presented to participants through a Head-Mounted Display (HMD) while performing a set of maneuvers. Each maneuver spanned one of the robot's DoF, had a duration of 6 seconds, and during its transition an arrow was visualized in the turning direction to aid the user's perception (Fig. 1B). We asked them to move their upper body in the same way they would if they were in control of the robot motion as they were seeing in the simulation. The participants were aware of the type of robot they were about to receive information from and did not receive further instructions.

A Motion Capture System (MoCap) was used to acquire human motion data modeling the upper body as a kinematic chain consisting of 9 rigid bodies. The resulting dataset, composed of the robot's control inputs and the pose (position and orientation) of the 9 rigid bodies representing the human upper body was then downsampled to a frequency of 100Hz and stored for subsequent analysis. Previous studies focused on spontaneous human motion patterns for the case of a fixed-wing drone flying at constant speed[10,28]. In order to compare our results with the existing literature, we also extended our dataset to include this robot. The 2-DoF fixed-wing data were obtained by selecting a subset of the fixed-wing drone data, excluding the speed-varying maneuvers. For the rest of this paper, we denote with $[x_R, y_R, z_R, \varphi_R, \theta_R, \psi_R]$ the pose of the robot R, with

$R \in [FF, F, Q, M]$ corresponding to the fixed-wing drone with constant speed, the fixed-wing drone with controlled speed, the quadrotor drone, and the manipulator, respectively.

Robot morphology and motion affects participants' interaction patterns

Our first results concern the analysis of the subjects' motion during the imitation task. We observed that the number of relevant body segments increases with the robot's complexity, i.e. the number of DoF. While only torso motion can be sufficient to control a drone, up to 6 segments are needed to control the manipulator (see Supplementary Material). Moreover, our data show that inter-subject motion variability, measured through the deviation from the median behavior[38], can increase up to 542% from a simple (FF) to a complex (M) robot (see Supplementary Material).

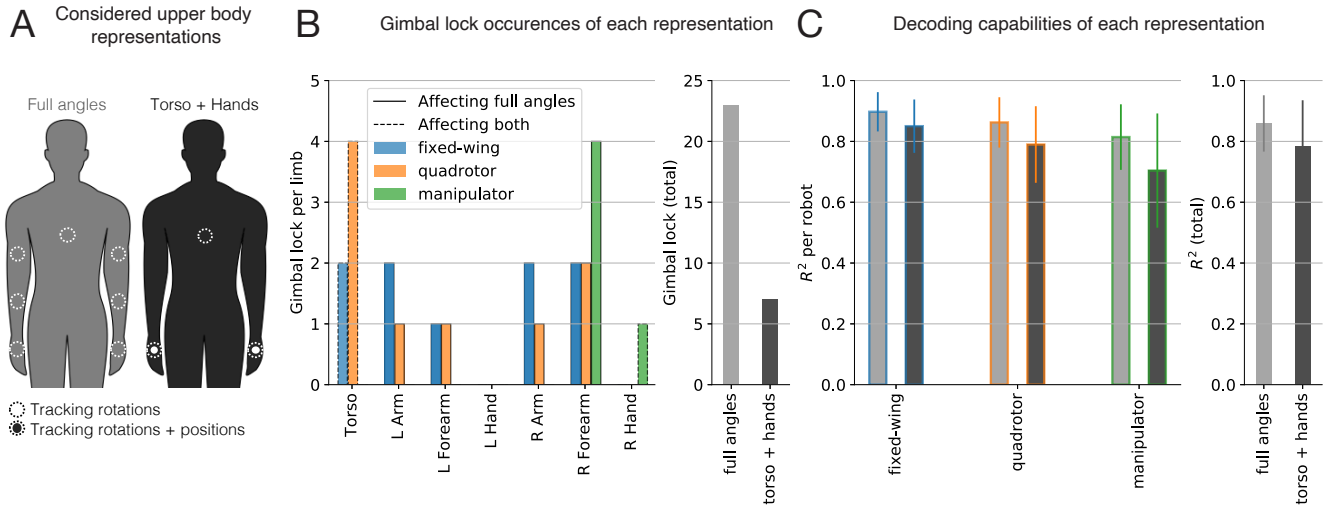

Figure 2. Comparison of full upper-body angles and torso+hands representations. (A) Schematic of the tracked body segments for the two models. (B) Number of datasets reaching a configuration close to gimbal lock singularity, divided by body segment (left) and total (right) for the two models. (C) Decoding capability of the two models in terms of regression R^2 score, divided by robot (left) and total (right). Torso+hands representation could avoid 70% of gimbal lock occurrences, while preserving 91.2% of the dataset's decoding capability.

Alternative body model reduces gimbal lock problem while retaining relevant information

Many studies model the human body as a concatenation of a set of rigid bodies, and consider their 3D rotations as kinematic variables, often with an Euler angles representation (we will call this model *full angles representation*)[28,39,40]. Such representation is susceptible to gimbal lock problems, which can in turn affect regression if close to singularities. 23 datasets (out of the total 30: 10 subjects for 3 robots) were close to gimbal lock during the imitation experiment (Fig. 2B). 16 of them were relative to the motion of arms and forearms, the body segments with the largest range of motion in the upper body[41–43]. To avoid this problem, we substituted the Euler angles associated to arms and forearms with the position of the user's hands in our dataset leading to a new reduced representation (Fig. 2A) that includes only the torso angle and the pose of the hands for a total of 15 kinematic variables (from now denoted as *torso+hands representation*). We denote with $[x_S, y_S, z_S, \varphi_S, \theta_S, \psi_S]$ the pose of the body segment $S \in [T, RH, LH]$ for torso, right hand, and left hand, respectively. Our data show that only 7 datasets out of 30 are affected by gimbal lock when considering the torso+hands model (Fig. 2B). We ran least-squares regression on the two different body models using as target values the robots' actions, observed a regression performance difference of 8.8% (Fig. 2C). This minor performance drop, along with the 70% augmented resilience to gimbal lock, demonstrates the effectiveness of the torso+hands representation. For this reason, we use this representation in the rest of the paper.

Synergy-aware mapping generation

Among other methods, PCA has shown to be efficient in identifying motor synergies[44–46]. Based on this knowledge, we first validated its effectiveness in identifying human motion synergies for robot teleoperation (see Supplementary Text), and then developed our synergy-aware mapping generation algorithm. We first extract one synergy per each of the robot's DoF using PCA, and later use them as regression variables (Fig. 3A-C, example for the fixed-wing drone). Unlike Principal Component Regression (PCR), we apply PCA on the time interval corresponding to each DoF separately, to remove the influence of the

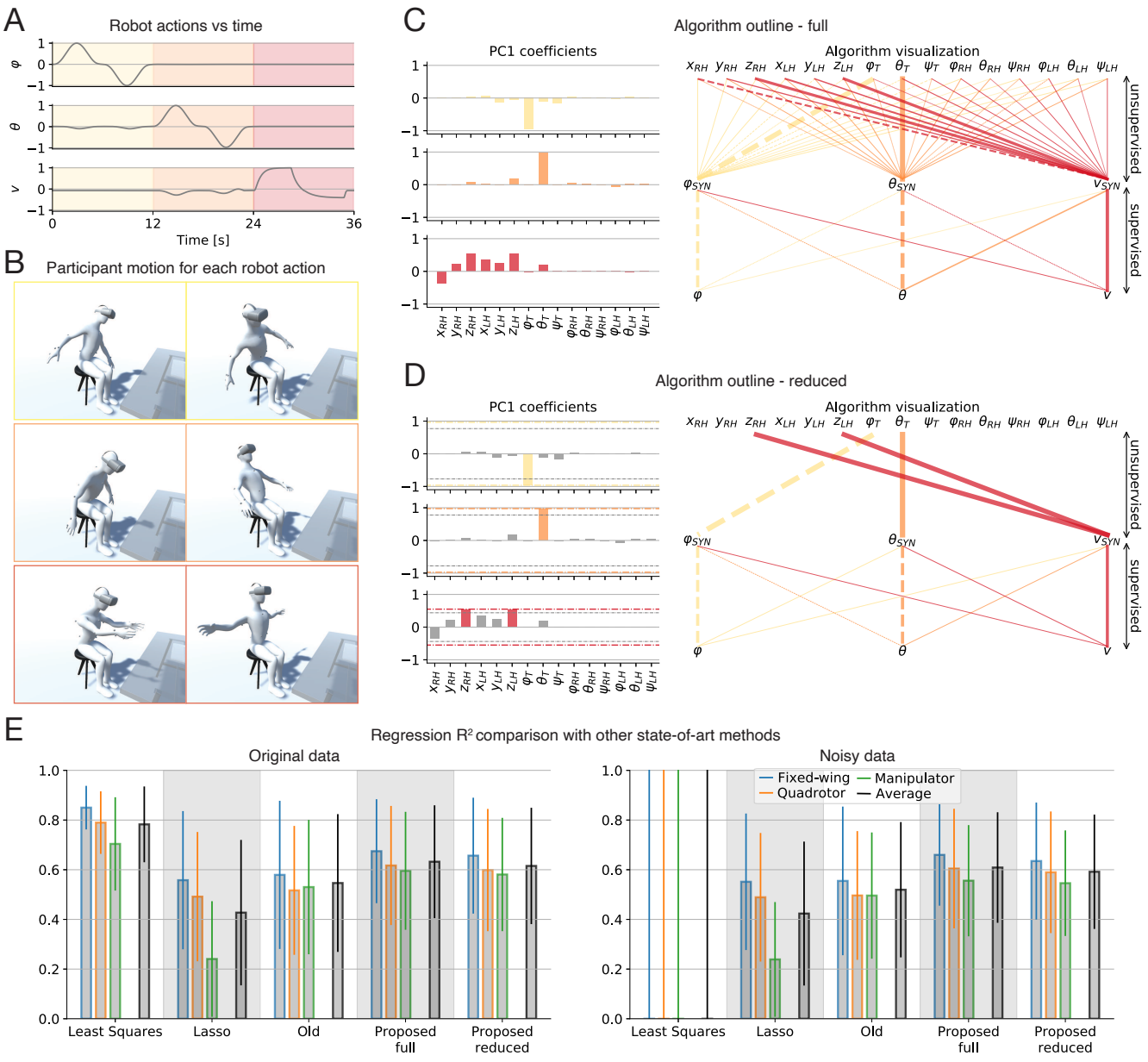

Figure 3. Algorithm outline - example data for the fixed-wing drone robot with variable speed - and offline performance evaluation. (A) Robot actions during the imitation task. The three DoFs change independently. (B) Human motion patterns relative to each robot action. The participant used torso motion to control roll (φ) and pitch (θ), and arms motion to control the speed (v). (C) Algorithm outline without feature selection (full). PC1 coefficients are used to define the three control synergies through unsupervised learning. The synergies are then regressed over the robot actions. (D) Algorithm outline with feature selection (reduced, k = 80%). Only the coefficients of PC1 over k% of the maximum value are retained. (E) Regression performance evaluation through R^2 score. Simple least squares regression overfits the data, showing $R^2 < 0$ for datasets with artificial noise, while the remaining methods show good regularization performance. The proposed method performs 30.4% better than Lasso and 14.7% better than our previous method. Feature selection reduces R^2 by 2.8%.

remaining maneuvers, which allows us to identify one motion synergy for each of the robot's DoFs (Fig. 3C). Thanks to this unsupervised dimensionality reduction step, our method prevents the regressor from overfitting while guaranteeing the compressed data to be functional, natural human synergies (see Video S10). Moreover, differently from other algorithms, the proposed method does not require any parameter tuning, which can be a complicated process sometimes carried out through

iterative optimization methods[34]. Finally, although the assumption of correlation between the first PC and the robot actions might seem limiting, we can use this parameter to assess the quality of the dataset, and possibly to repeat the imitation phase.

We evaluated two versions of our method: the first one integrates the full set of kinematic variables into a synergy through PCA coefficients, while the second one performs feature selection by only considering kinematic variables having sufficiently high coefficients by setting a threshold value (Fig. 3D, see Materials and Methods). We will refer to the two methods as *reduced* and *full* versions.

We compared the proposed method with state-of-the-art regression methods used for body motion processing: linear regression, lasso, and our previously proposed algorithm (Fig. 3E)[28,34]. We added artificial noise to the data ($std = 1cm$ for the linear variables, $std = 1^\circ$ for the angular variables) to assess the regularization effectiveness. Our results show that, for non-noisy data, least squares regression provides the best results, with a R^2 score outperforming Lasso regression by 45.4%, our old method by 30.2%, and our new method by 19.2% and 21.4%, for the full and reduced versions, respectively. However, the high least squares performance is due to overfitting, as demonstrated by the negative R^2 obtained on noisy data. Oppositely, all the alternative methods could cope with the noisy dataset with a low performance drop: 0.9% for Lasso, 4.9% for our old method, and 3.7% and 3.8%, for the new full and reduced methods, respectively. Out of the regularized methods, our proposed algorithm performed the best ($R^2_{NEW} = 0.61 \pm 0.22$), followed by the old ($R^2_{OLD} = 0.52 \pm 0.27$) and Lasso ($R^2_{LASSO} = 0.42 \pm 0.29$). Feature selection only reduced the performance by 2.8% ($R^2_{NEW\_REDUCED} = 0.59 \pm 0.23$).

Results

We ran a user study to assess the effectiveness of the proposed method for personalized human-robot interface generation. 18 subjects took part in the study, and were asked to teleoperate one of the three robots in a simulated environment (6 subjects per robot). Each participant controlled the robot with a personalized human-robot interface based on the synergy-aware mapping generation algorithm and with a standard remote. Later, also the full version of the body-machine interface was tested. Hereafter, the three groups are referred to as group R for remote, group M for motion, and group MF for the motion-based full interface. Task and performance metric were robot-dependent: for the flying robots we implemented a navigation task, while for the manipulator we simulated a peg-in-hole task (Fig. 4A, see Materials and Methods for further details, and Videos S4, S5, S6). Finally, the participants filled in a questionnaire composed of the NASA-TLX test to evaluate their cognitive workload, and a personal user experience form (Materials and Methods).

Personalized BoMI performs similarly or better than remote

We examined the users' performance in the different tasks to validate our interface generation method. All the subjects were able to complete their task, as a demonstration of the usability of our method. Fixed-wing pilots could attain significantly lower error when piloting the drone through their personalized body motion (Fig. 4B-C). In particular, group R showed a higher error score both before ($err_{R-B} = 4.31 \pm 3.52m$) and after training ($err_{R-A} = 3.52 \pm 2.99m$) than group M ($err_{M-B} = 2.29 \pm 1.54m, p < 0.01$ and $err_{M-A} = 1.93 \pm 1.19m, p < 0.01$), and an average error increase of 93.5% ($p < 0.01$) over the two runs. Quadrotor pilots, contrarily, performed better using the joystick (Fig. 4D-E). Group R took less time ($t_R = 7.38 \pm 5.48s$) than group M to navigate through the waypoints ($t_M = 8.33 \pm 5.06s$), saving on average 11.4% of time. However, group M started with better performance ($t_{M-B} = 8.12 \pm 4.83s$) than group R ($t_{R-B} = 8.75 \pm 6.55s$), but did not improve between runs, while group R improved by 32.6% ($p < 0.01$) . Finally, operating the manipulator, group M performed again better than group R (Fig. 4F-G). On average, using a personalized motion-based interface reduced the time needed to complete the peg in hole task by 41.9% ($t_M = 10.86 \pm 4.48s, t_R = 18.68 \pm 12.21s, p < 0.01$). Group M outperformed group R both before ($t_{M-B} = 11.33 \pm 4.81s, t_{R-B} = 17.41 \pm 9.96s, p < 0.01$) and after training ($t_{M-A} = 10.29 \pm 3.98s, t_{R-A} = 17.37 \pm 11.29s, p < 0.01$).

Users reported to prefer BoMI over remote

First, we describe the results of the NASA-TLX questionnaire (Fig. 5A). On average, group M found the task less mentally demanding ($QN1_M = 44.67 \pm 18.58$) than groups R ($QN1_R = 62.28 \pm 17.20, p = 0.013$) and MF ($QN1_{MF} = 63.89 \pm 24.64, p = 0.030$). In turn, the remote was considered less physically demanding ($QN2_R = 32.78 \pm 21.96$) than the two BoMIs ($QN2_M = 50.61 \pm 18.79, p = 0.044, QN1_{MF} = 55.78 \pm 19.60, p < 0.01$). Finally, subjects in group M felt to have been more successful and less rushed ($QN4_M = 75.56 \pm 19.62, QN5_M = 26.17 \pm 17.59$) than remote users ($QN4_R = 62.00 \pm 24.97, p = 0.025, QN5_R = 39.39 \pm 19.11, p = 0.046$). Most subjects (14 out of 18) preferred the motion-based interface to carry out the task. Specifically, only two subjects controlling the quadrotor and two controlling the manipulator preferred the remote controller. The participants described the BoMI to be more intuitive and the related experience to be more enjoyable, as they had to focus less on the meaning of each movement to control the robot.

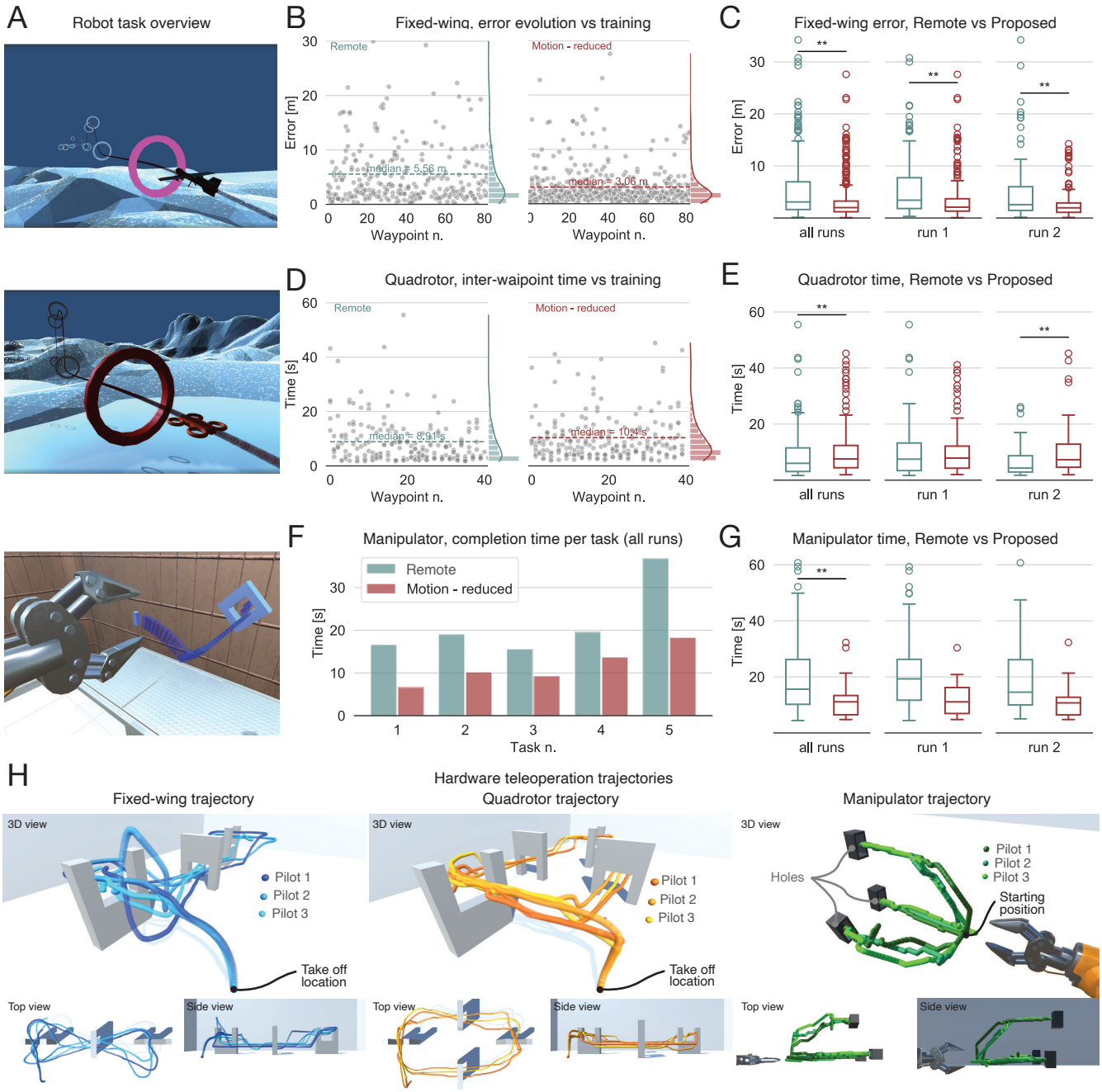

Figure 4. Simulated and hardware validation of the proposed method. (A) Third-person overview of the task: navigation for fixed-wing and quadrotor, peg-in-hole for manipulator. (B) Error evolution over training for fixed-wing drone navigation. (C) Comparative boxplot for motion-based and remote teleoperation for the fixed-wing drone. Group M outperformed group R both before and after training, reducing errors by 48.3% on average. (D) Time evolution over training for quadrotor drone navigation. (E) Comparative boxplot for motion-based and remote teleoperation for the quadrotor drone. Group M outperformed group R by 7.2% before training. However, trained users performed better with the remote. On average, group R needed 11.4% less time. (F) Time needed to complete the peg-in-hole task for each hole placement (6 subjects per 5 peg-in-hole tasks). Group M reached higher performance in all iterations for all the holes. (G) Comparative boxplot for motion-based and joystick teleoperation for the manipulator. Group M outperformed group R both before and after training, reducing the time needed to complete the tasks by 41.2% on average. (H) 3D reconstruction of the real drones' and the manipulator's trajectories. All subjects (N=9) managed to successfully accomplish the task.

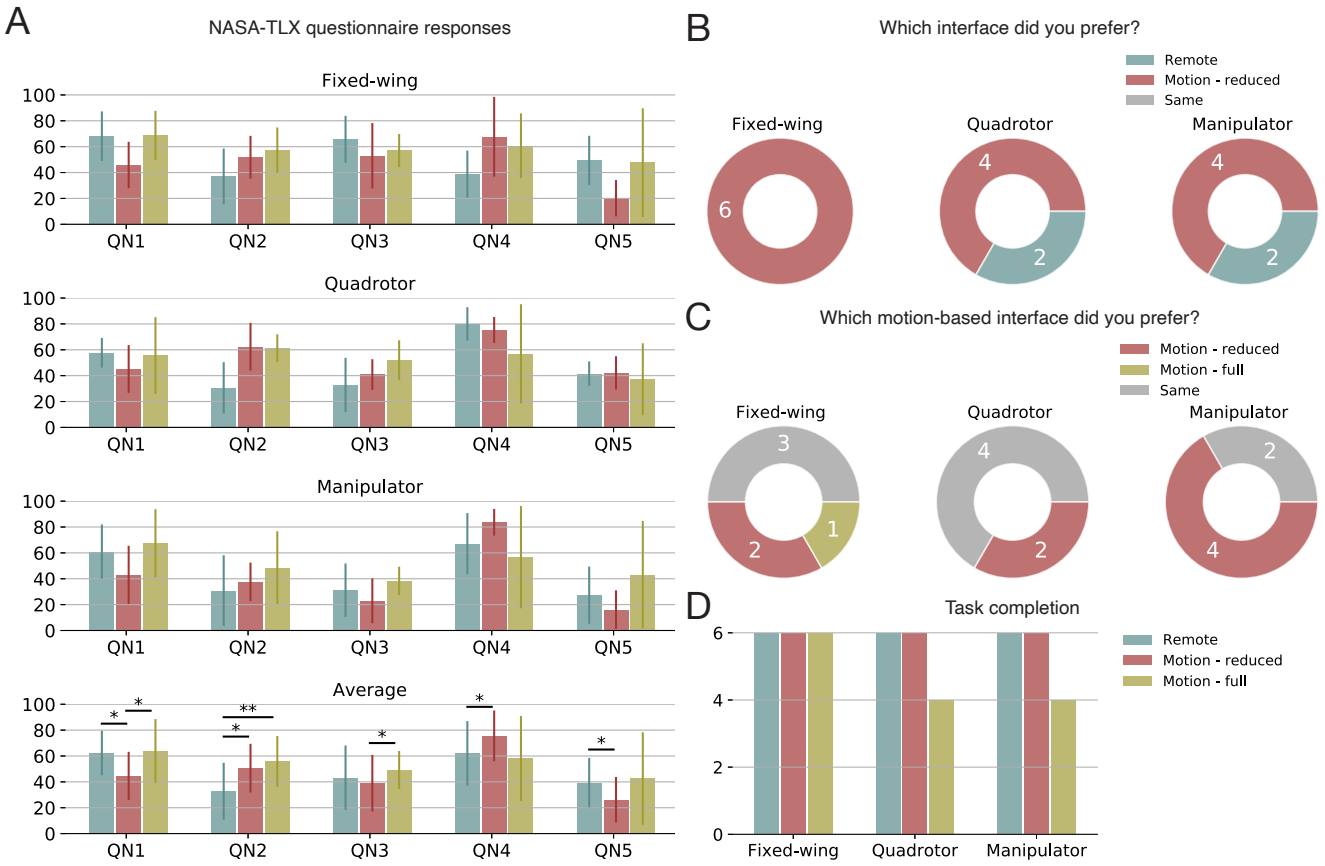

Figure 5. Survey results and task completion for the simulated teleoperation experiment. (A) NASA-TLX responses for the three robots. On average, the use of the reduced motion-based interface resulted in a lower mental workload, while the remote provided less physical workload. (B) Preference indications between remote and BoMI. Most participants (14/18) preferred the BoMI. (C) Preference indications between reduced and full BoMI. Only one participant (fixed-wing user) preferred the full version (D) Task completion per robot. Two participants for the quadrotor and 2 for the manipulator could not complete the task using the full BoMI.

Feature selection can be essential to the usability of BoMIs

When asked to indicate their preferred motion-based interface, 9 out of 18 participants reported to have found no difference between the two while 8 out of 18 preferred the reduced BoMI (Fig. 5C). In particular four subjects, two in the quadrotor group and two in the manipulator group, were not able to complete the given task using the BoMI without feature selection, reporting later that it was “impossible to use” (Fig. 5D).

Teleoperation of real robots

We executed a set of experiments on real robots to validate the effectiveness of our method. 9 additional participants (3 per robot) were recruited to participate in this phase. The experiments were aimed at reproducing, in a real-world controlled environment, teleoperation tasks similar to the ones presented in simulation. Drone navigation was performed through a set of gates arranged in the MoCap room, while manipulator operation was carried out on the real robot (see Materials and Methods, Supplementary Text and Videos S7, S8, S9). All participants were able to successfully complete the given task with 0 accidents (Fig. 4H).

Discussion

This work describes new results about human’s spontaneous motor behaviour for robot imitation, and builds on this knowledge for the development of a novel machine learning algorithm for automated body-machine interface generation.

Our first results concern the observation of the interaction strategies of users when approaching different robots in an

imitation task (see Supplementary Text). We observed that the number of body segments involved increased with the increase of the number of DoF of the robot (Suppl. Fig. S1B). The use of additional limbs is not based on an innate preference, but it rather depends on the knowledge of the users about the type of robot to control (e.g., knowing the manipulator's morphology persuaded our users to imitate its motion with their arms). Indeed, despite the similarity in the DoFs of the quadrotor and the manipulator in our imitation task, participants moved mostly their torso to imitate the first robot and mostly their arms to imitate the second one. Also, we found that humans tend to move their body more similarly with each other when imitating simple robots, and present a higher variability when imitating robots with a higher number of DoF (Fig. S1E), thus requiring a higher level of personalization.

A problem when using Euler angles when designing BoMIs is gimbal lock. The majority of our subjects (23 out of 30 participants) moved to near-singularity positions during the task (Fig. 2B). The new representation proposed here (Fig. 2A) reduced by 70% gimbal lock occurrences while preserving 91.2% of the dataset's relevant information (Fig. 2B-C).

Our correlation study between human and robot motion demonstrated that appropriate dimensionality reduction methods can be employed to simplify a motion dataset into a set of human motion synergies (Suppl. Fig.S2). By applying PCA to the motion data we discovered that, for this kind of imitation task, the majority of the dataset's information (>80%) can be compressed into a single variable through linear projection (Suppl. Fig.S2B). Based on the latter result, we designed a novel synergy-aware regression algorithm to map the user's movement into robot commands (Fig. 3). Our algorithm first generates one motion synergy for each of the robot's DoFs through unsupervised learning, then performs linear regression on the set of synergies (Fig. 3C-D). We developed two versions of the algorithm: the first version considers all the kinematic variables to define the synergies through PCA (Fig. 3C), while the second (reduced) version selects only the most relevant ones, based on their projection coefficients (Fig. 3D). We showed that the method proposed here, through the unsupervised dimensionality reduction step, can prevent overfitting like established regularization methods (Fig. 3E) and outperform state-of-the-art methods (Fig. 3F).

The interfaces generated through the reduced method demonstrated to be usable and effective. All subjects (N=18) managed to operate the robots to complete the given tasks (Fig. 4). Personalized BoMIs reduced their error in fixed-wing navigation by 48.3% and the time needed for a peg-in-hole task with the manipulator by 41.2% (Fig. 4B-G). Contrarily, quadrotor navigation took 11.2% less time to remote controller users (Fig. 4E). However, subjects performed better on average before training when using the BoMI than the remote, suggesting that generating commands for the robot based on their individual preference allowed them to get proficient more quickly, in accordance with prior literature[28]. Accordingly, users reported to prefer to use a BoMI in terms of user experience (Fig. 5B), which might be due to the lower perceived mental demand (Fig. 5A).

When using the full version of the algorithm, 4 out of 18 subjects could not replicate the same performance and had to stop the experiment, as the interface was defined as "unusable" (Fig. 5D). However, the regression R^2 was similar in the two cases. This result suggests that regression performance is not necessarily a good predictor for BoMI implementation, and it should not be considered as a sufficient metric to optimize their design. More specifically, this result opens to considerations on the structural organization of human motion synergies. The inability to use the full version of the interface suggests that human motion is structured to consider specific elements of a synergy and that they are not, in principle, capable of reproducing accurately even the patters identified by the first principal component.

This work opens to interesting future investigations on body-motion based robot teleoperation systems. First, the proposed BoMIs were fixed by the regression algorithm and could not be changed at operation time. As the user might present different cognitive or physical workload levels during the operation, or might get injured, an adaptive interface that changes according to these factors could solve the problem. Also, despite the significant differences in the morphology and the DoFs of the considered robots, the control more articulated machines (such as legged robots, or humanoids) could require the regression between motor synergies for both the human and the robot, thus allowing the fine operation of complex structures at once.

Materials and Methods

Imitation task - experimental protocols

The robot imitation task was performed by all subjects taking part in the motion acquisition stage, in the teleoperation of simulated robots, and in the hardware experiments. Robot maneuvers were presented in FPV to the user through an HMD (Fig. 1A), while a red arrow pointing in the direction of the robot's motion was displayed to aid their perception. T ensure maneuver continuity, we sent continuous control signals to the simulator following the formula $input = \frac{A}{2}\left(1-\left(cos\left(\frac{t2\pi}{T}\right)\right)\right)$ (for further details see Supplementary Material).

Reduced-full version of the algorithm

The reduced version of the algorithm removes most of the initially acquired kinematic variables, retaining the most significant ones and resulting in a simplified motion synergy (see supplementary video). The PCA coefficients are finally re-normalized so that $\xi_i^2 = 1$, where ξ_i is the coefficient associated with the $i-th$ kinematic variable of PC1.

Teleoperation - experimental protocols

Simulation experiments

Each participant performed the imitation task as described above, and we provided them with a personalized human-robot interface by using the proposed synergy-aware mapping generation algorithm. Since the considered robots are morphologically and dynamically different, both the task and the performance metric were robot-dependent. Fixed-wing and quadrotor users had to perform a navigation task through a predefined path. The path consisted of a set of circular waypoints (Fig. 4A). The waypoints were placed in such a way that 3D navigation was required, so to activate the highest possible number or robot DoFs simultaneously. Moreover, the inter-waypoint distance for the fixed-wing path was set to require the user to actively control the flight speed in some segments. Since the flight of the fixed-wing drone could not be stopped, we evaluate the precision of the navigation in terms of error when hitting a waypoint plane, even if the waypoint was not hit correctly. The error was defined as the distance between the drone and the center of the waypoint at the moment when the drone crossed the circle's plane. Since the quadrotor drone could be stabilized to hover without moving, an error metric would not reflect a good control capability, as a user might take a very long time to align with the waypoint center. In this case, we used the inter-waypoint navigation time as a performance metric and required each waypoint to be hit correctly. Finally, the manipulator users had to complete a peg-in-hole task. We asked them to operate the robot to fit a prismatic peg in a set of holes placed in different positions and orientations (Fig. 4A). The user was required to hold the peg statically inside the hole for 3 seconds before the task was considered complete. We evaluated the participants' performance based on the total time needed to complete the task. The tasks were performed both with an interface generated by the proposed algorithm (reduced version) and with a standard remote controller. The starting interface was chosen pseudo-randomly. Later, also the full version of the body-machine interface was tested. The starting interface was determined pseudo-randomly for each user. To quantify the learning capabilities of our participants in using the two interfaces, all of them had to repeat the task twice. After the teleoperation task, our participants were asked to fill in a questionnaire comprising two sections: the NASA-TLX to evaluate their load index, and an additional subjective questionnaire regarding their user experience using the different interfaces (Tab. 1).

ID	Question
QN1	How mentally demanding was the experiment?
QN2	How physically demanding was the experiment?
QN3	How hurried or rushed was the pace of the task?
QN4	How successful were you in accomplishing the task?
QN5	How insecure, stressed, irritated, and annoyed were you?
Q6	Which interface did you prefer?
Q7	Which motion-based interface did you prefer?

Table 1. User personal feedback questionnaire.

Hardware experiments

Fixed-wing teleoperation: the flight of the fixed-wing was set to a nominal speed of $0.2m/s$, controllable in the range 0.1-0.3m/s. The task was implemented on a quadrotor drone, which control system was set to reproduce a fixed-wing-like flight[47].
Quadrotor teleoperation: the task was implemented on the same robot, with standard quadrotor dynamics. Two different paths were realized in the MoCap room using a set of obstacles (see Supplementary Text and Video). Each participant was asked to navigate through the path once. The communication between the PC and the quadrotor (Crazyflie 2.1) was implemented through ROS and the Crazyswarm library[48].
Quadrotor teleoperation: the peg-in-hole task was performed using a Stäubli TX2-90 manipulator, and participants were asked to insert the end-effector in a small box measuring $5.8x3.6cm$ (see Supplementary Text and Video). The communication between the PC and the manipulator RoboDK and the Robolink library[1].

Participants

10 participants (26.2 $\pm$ 2.1 years old, 2 females) took part in the motion acquisition experiment. Their motion was recorded along with the simulation data for further analysis and the offline validation of our algorithm. We instructed them to move according to the visualized robot maneuvers and displayed arrows, no further instructions were provided. 18 participants (25.6 $\pm$ 1.8 years old, 5 females) were recruited for the teleoperation experiment in simulation. Divided into 3 groups (1 per robot), they were first instructed to imitate the robot's motion as in the previous phase, and later explained the goal of the task. Finally, 9 participants (25.8 $\pm$ 2.3 years old, 1 female) took part into the final real-world experiment. Analogously with the

[1] https://robodk.com/index

second group, they performed the imitation task and later the teleoperation task. The experiments were approved by the École Polytechnique Fédérale de Lausanne Human Research Ethics Committee.

Acknowledgments

This work was partially funded by the European Union's Horizon 2020 research and innovation programme under grant agreement ID: 871479 AERIAL-CORE, the Swiss National Science Foundation (SNSF) with grant number 200021-155907, and the National Centre of Competence in Research (NCCR) Robotics.

References

1. Niemeyer, G., Preusche, C., Stramigioli, S. & Lee, D. Telerobotics. In Siciliano, B. & Khatib, O. (eds.) *Springer Handbook of Robotics*, 1085–1108 (Springer, Berlin, Heidelberg, 2016).

2. Abbink, D. A. *et al.* A topology of shared control systems—finding common ground in diversity. *IEEE Trans. Hum. Mach.Syst* **48**, 509–525, DOI: 10.1109/THMS.2018.2791570 (2018).

3. Nagatani, K. *et al.* Emergency response to the nuclear accident at the fukushima daiichi nuclear power plants using mobile rescue robots: Emergency response to the fukushima nuclear accident using rescue robots. *J. Field Robotics* **30**, 44–63, DOI: 10.1002/rob.21439 (2013).

4. Taylor, R. & Stoianovici, D. Medical robotics in computer-integrated surgery. *IEEE Trans. Robot. Autom.* **19**, 765–781, DOI: 10.1109/TRA.2003.817058 (2003).

5. Murphy, R. R. *et al.* Search and rescue robotics. In *Springer Handbook of Robotics*, 23 (2008).

6. Murphy, R. Human–robot interaction in rescue robotics. *IEEE Trans. Syst., Man, Cybern. C* **34**, 138–153, DOI: 10.1109/TSMCC.2004.826267 (2004-05).

7. Casper, J. & Murphy, R. Human-robot interactions during the robot-assisted urban search and rescue response at the world trade center. *IEEE Trans. Syst., Man, Cybern.* **33**, 367–385, DOI: 10.1109/TSMCB.2003.811794 (2003).

8. Herder, J. L., Vrijlandt, N., Antonides, T., Cloosterman, M. & Mastenbroek, P. L. Principle and design of a mobile arm support for people with muscular weakness. *J. Rehabil. Res. Dev.* **43**, 591, DOI: 10.1682/JRRD.2006.05.0044 (2006).

9. Chen, J. Y. C., Barnes, M. J. & Harper-Sciarini, M. Supervisory control of multiple robots: Human-performance issues and user-interface design. *IEEE Trans. Syst., Man, Cybern. C* **41**, 435–454, DOI: 10.1109/TSMCC.2010.2056682 (2011).

10. Miehlbradt, J. *et al.* Data-driven body–machine interface for the accurate control of drones. *Proc. Natl. Acad. Sci.* **115**, 7913–7918, DOI: 10.1073/pnas.1718648115 (2018).

11. Seanez-Gonzalez, I. *et al.* Static versus dynamic decoding algorithms in a non-invasive body–machine interface. *IEEE Trans. Neural Syst. Rehabil. Eng.* **25**, 893–905, DOI: 10.1109/TNSRE.2016.2640360 (2017-07).

12. Pierella, C. *et al.* Remapping residual coordination for controlling assistive devices and recovering motor functions. *Neuropsychologia* **79**, 364–376, DOI: 10.1016/j.neuropsychologia.2015.08.024 (2015).

13. LaFleur, K. *et al.* Quadcopter control in three-dimensional space using a noninvasive motor imagery-based brain–computer interface. *J. Neural Eng.* **10**, 046003, DOI: 10.1088/1741-2560/10/4/046003 (2013).

14. Kim, B. H., Kim, M. & Jo, S. Quadcopter flight control using a low-cost hybrid interface with EEG-based classification and eye tracking. *Comput. Biol. Med.* **51**, 82–92, DOI: 10.1016/j.compbiomed.2014.04.020 (2014).

15. Song, X. *et al.* A quadcopter controlled by brain concentration and eye blink. In *IEEE Sig. Proc. Med. Bio. (SPMB)*, 1–4, DOI: 10.1109/SPMB.2016.7846875 (IEEE, 2016).

16. Casadio, M., Ranganathan, R. & Mussa-Ivaldi, F. A. The body-machine interface: A new perspective on an old theme. *J. Mot. Behav.* **44**, 419–433, DOI: 10.1080/00222895.2012.700968 (2012).

17. Gromov, B., Gambardella, L. M. & Giusti, A. Robot identification and localization with pointing gestures. 3921–3928, DOI: 10.1109/IROS.2018.8594174 (IEEE, 2018).

18. Gromov, B., Abbate, G., Gambardella, L. M. & Giusti, A. Proximity human-robot interaction using pointing gestures and a wrist-mounted IMU. In *IEEE Intl. Conf. on Rob. and Aut. (ICRA)*, 8 (2019).

19. Sanna, A., Lamberti, F., Paravati, G. & Manuri, F. A kinect-based natural interface for quadrotor control. *Entertain. Comput.* **4**, 179–186, DOI: 10.1016/j.entcom.2013.01.001 (2013).

20. Pfeil, K., Koh, S. L. & LaViola, J. Exploring 3d gesture metaphors for interaction with unmanned aerial vehicles. In *IEEE Intl. Conf. on Intell. User Interf. (IUI)*, 257, DOI: 10.1145/2449396.2449429 (ACM Press, 2013).

21. Ambrose, R. *et al.* Robonaut: NASA's space humanoid. *IEEE Intell. Syst.* **15**, 57–63, DOI: 10.1109/5254.867913 (2000).

22. Fukuda, O., Tsuji, T., Kaneko, M. & Otsuka, A. A human-assisting manipulator teleoperated by EMG signals and arm motions. *IEEE Trans. Robot. Autom.* **19**, 210–222, DOI: 10.1109/TRA.2003.808873 (2003).

23. Melidis, C., Iizuka, H. & Marocco, D. Intuitive control of mobile robots: an architecture for autonomous adaptive dynamic behaviour integration. *Cogn Process.* **19**, 245–264, DOI: 10.1007/s10339-017-0818-5 (2018).

24. Pierce, R. M. & Kuchenbecker, K. J. A data-driven method for determining natural human-robot motion mappings in teleoperation. In *2012 4th IEEE/EMBS Intl. Conf. on Biomed.l Rob. and Biomech. (BioRob)*, 169–176, DOI: 10.1109/BioRob.2012.6290927 (2012).

25. Cauchard, J. R., E, J. L., Zhai, K. Y. & Landay, J. A. Drone & me: an exploration into natural human-drone interaction. In *ACM Intl. Conf. on Pervasive and Ubiquitous Computing (UbiComp)*, 361–365, DOI: 10.1145/2750858.2805823 (2015).

26. Melidis, C. & Marocco, D. KURE: Kinematic universal remote interface a human centred remote robot control paradigm. In *IEEE Intl.Conf. Syst., Man, Cybern. (SMC)*, 3130–3135, DOI: 10.1109/SMC.2016.7844716 (IEEE, 2016).

27. Khurshid, R. P. & Kuchenbecker, K. J. Data-driven motion mappings improve transparency in teleoperation. *Presence* **24**, 132–154, DOI: 10.1162/PRES_a_00223 (2015).

28. Macchini, M., Schiano, F. & Floreano, D. Personalized telerobotics by fast machine learning of body-machine interfaces. *IEEE Rob. Autom. Lett.* **5**, 179–186 (2020).

29. Leo, A. *et al.* A synergy-based hand control is encoded in human motor cortical areas. *eLife* **5**, e13420, DOI: 10.7554/eLife.13420 (2016).

30. Stergiou, N. & Decker, L. M. Human movement variability, nonlinear dynamics, and pathology: Is there a connection? *Hum. Mov. Sci.* **30**, 869–888, DOI: 10.1016/j.humov.2011.06.002 (2011).

31. Winter, D. A. *The biomechanics and motor control of human gait* (Univ. of Waterloo Press, 1987).

32. Alessandro, C., Delis, I., Nori, F., Panzeri, S. & Berret, B. Muscle synergies in neuroscience and robotics: from input-space to task-space perspectives. *Front. Comput. Neurosci.* **7**, DOI: 10.3389/fncom.2013.00043 (2013).

33. Ferrignoa, G. Pattern recognition in 3D automatic human motion analysis. *J. Photogramm.* 20 (1990).

34. Hans, C. Bayesian lasso regression. *Biometrika* 11 (2009).

35. Ficuciello, F., Falco, P. & Calinon, S. A Brief Survey on the Role of Dimensionality Reduction in Manipulation Learning and Control. *IEEE Robot. Autom. Lett.* **3**, 2608–2615, DOI: 10.1109/LRA.2018.2818933 (2018).

36. Seáñez-González, I. & Mussa-Ivaldi, F. A. Cursor control by kalman filter with a non-invasive body–machine interface. *J. Neural Eng.* **11**, 056026, DOI: 10.1088/1741-2560/11/5/056026 (2014).

37. Rizzoglio, F., Casadio, M., De Santis, D. & Mussa-Ivaldi, F. A. Building an adaptive interface via unsupervised tracking of latent manifolds. *Neural Networks* **137**, 174–187, DOI: 10.1016/j.neunet.2021.01.009 (2021).

38. Macchini, M., Lortkipanidze, M., Schiano, F. & Floreano, D. The Impact of Virtual Reality and Viewpoints in Body Motion Based Drone Teleoperation. In *IEEE Virtual Reality (VR)*, 511–518 (2021).

39. Kamel, A., Sheng, B., Li, P., Kim, J. & Feng, D. D. Efficient body motion quantification and similarity evaluation using 3-d joints skeleton coordinates. *IEEE Trans. Syst. Man Cybern, Syst.* 1–15, DOI: 10.1109/TSMC.2019.2916896 (2019).

40. Farshchiansadegh, A. *et al.* A body machine interface based on inertial sensors. In *Intl. Conf. Med. Bio. (EMBS)*, 6120–6124, DOI: 10.1109/EMBC.2014.6945026 (IEEE, 2014).

41. Macchini, M., Frogg, J., Schiano, F. & Floreano, D. Does spontaneous motion lead to intuitive Body-Machine Interfaces? A fitness study of different body segments for wearable telerobotics. *IEEE Intl. Conf. Rob. Hum. Inter. Comm. (RO-MAN)* (2020).

42. Boone, D. C. & Azen, S. P. Normal range of motion of joints in male subjects.:. *J. Bone Jt. Surg.* **61**, 756–759, DOI: 10.2106/00004623-197961050-00017 (1979).

43. Doriot, N. & Wang, X. Effects of age and gender on maximum voluntary range of motion of the upper body joints. *Ergonomics* **49**, 269–281, DOI: 10.1080/00140130500489873 (2006).

44. Gloersen, O. Technique analysis in elite athletes using principal component analysis. *J. Sports Sci.* 10 (2017).

45. Vasilescu, M. A. O. Human motion signatures: analysis, synthesis, recognition. In *Intl. Conf. Patt. Rec.*, 5 (2002).

46. Bokman Lim, Syungkwon Ra & Park, F. Movement primitives, principal component analysis, and the efficient generation of natural motions. 4630–4635, DOI: 10.1109/ROBOT.2005.1570834 (IEEE, 2005).

47. Cherpillod, A., Floreano, D. & Mintchev, S. Embodied flight with a drone. In *IEEE Intl. Conf. on Rob. Comp. (IRC)*, 386–390, DOI: 10.1109/IRC.2019.00070 (IEEE, 2019).

48. Preiss, J. A., Honig, W., Sukhatme, G. S. & Ayanian, N. Crazyswarm: A large nano-quadcopter swarm. 3299–3304, DOI: 10.1109/ICRA.2017.7989376 (2017).

49. Macchini, M., Schiano, F. & Floreano, D. Data-driven personalization of body-machine interfaces to control diverse robot types. *Zenodo* DOI: 10.5281/zenodo.5014111 (2021).

Code and data availability

Simulation and hardware experimental data that supports the findings of this study, along with the code used to process the data and generate the figures can be downloaded from[49].

Author contributions statement

M.M., F.S., and D.F. conceived the experiments; M.M. conducted the experiments; M.M. analyzed data; M.M. developed the simulators, the robots, and their control interfaces; and M.M., F.S., and D.F. wrote the paper.

Competing interests

The authors declare that they have no competing interests.

Supplementary Files

This is a list of supplementary files associated with this preprint. Click to download.

- SupplementaryMaterialDataDrivenPersonalizationofBodyMachineInterfacestoControlDiverseRobotTypes.pdf
- S1.mp4
- S2.mp4
- S3.mp4
- S4.mp4
- S5.mp4
- S6.mp4
- S7.mp4
- S8.mp4
- S9.mp4
- S10.mp4